ACS OMEGA

http://pubs.acs.org/journal/acsodf

Article

Juglans Sporopollenin for High-Performance Supercapacitor Electrode Design

Funda Ersoy Atalay,* Alper Bingol, Harun Kaya, Yıldız Emre, Hatice Hande Bas, and Ayse Asiye Culum

Cite This: *ACS Omega* 2020, 5, 20417−20427

Read Online

ACCESS | Metrics & More | Article Recommendations | Supporting Information

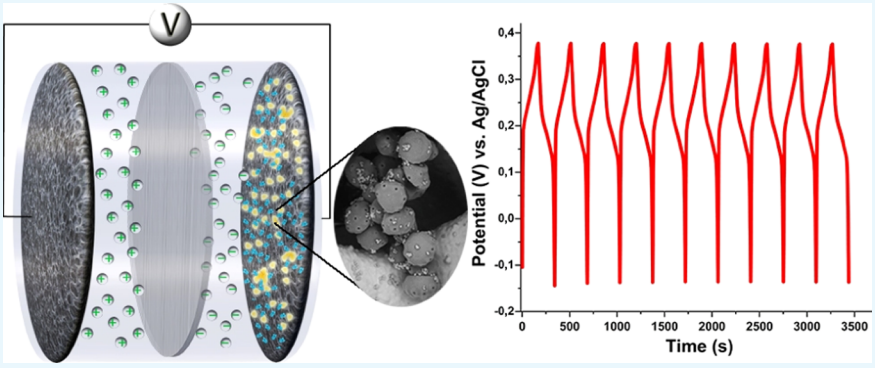

ABSTRACT: Recently, plant pollen has been used as a source of activated carbon to produce carbon-containing supercapacitor electrodes. However, in this study, pollen was used as a biotemplate with a completely different approach. As a biotemplate, pollen offers a wide range of varieties in terms of exterior, porosity, shape, and size. An electrode formed by the use of metal oxide grown on the pollen exine layer (sporopollenin microcapsules) as the active substance will inevitably exhibit good electrochemical capacitive properties. *Juglans* male flowers have been distinguished by dissection from anthers. Isolation of pollen grains from anthers was carried out using sieving from suitable sieves (45−200 μm). *Juglans* sporopollenin exine microcapsules (SECs) were separated from the intine and protoplasm by acetolysis in combination with reflux. The solution containing SECs, metal ions, and Ni foam was put into a Teflon-lined hydrothermal container, and then, it was reacted at 120 °C for 15 h. The resulting precipitate, as well as the Ni foam, was heat-treated at 300 and 360 °C for 3 h in air. The raw pollen, chemically treated pollen, and cobalt-coated SEC (CoSEC) and CoSEC/Ni foam were characterized using scanning electron microscopy, Brunauer−Emmett−Teller surface area analysis, thermogravimetric analysis, and X-ray diffraction techniques. Two different types of supercapacitor electrode designs, with the use of exine microcapsules of *Juglans* sporopollenin, were performed for the first time. The maximum specific capacitance was up to 1691 F g^{-1} at 5 A g^{-1}.

INTRODUCTION

Nanomaterials are the most studied models of matter in producing functional devices. Research on the production of nanostructured materials and their solution-oriented technological applications is rapidly increasing worldwide. These materials are beginning to be used technologically in different sectors, such as electronics, optics, textiles, medicine, and the environment. When a bulk material is reduced to the nanoscale, it acquires new technological features, such as unique optical, electrical, mechanical, and magnetic properties. Because of their high surface/volume ratio and excellent surface activity, nanostructured metal oxide/hydroxide materials, in particular, have found potential applications in many areas, including gas sensors[1] and biosensor applications,[2] energy storage[3] (as an electrode material), medicine[4] (in diagnosis and treatment), and many more. In many processes, from electrochemical processes to heterogeneous catalytic reactions on electrode surfaces, reactions on the surface (or interface) play a critical role.[5,6] Therefore, researchers prefer to synthesize small-sized nanomaterials to ensure exposure to larger surface areas. However, conventional nanoparticles are often unstable and tend to shrink further with reactions when their size is extremely small. This clustering of active materials on electrochemical electrodes (or catalysts) causes a decrease in the accessible surface area contributing to the reaction, which leads to a decrease in their activity.

Microcapsules of Sporopollenin as a Biotemplate. Plant pollen, a structure offered by nature, will be utilized to find

Received: May 20, 2020
Accepted: July 23, 2020
Published: August 6, 2020

https://dx.doi.org/10.1021/acsomega.0c02355
ACS Omega 2020, 5, 20417−20427

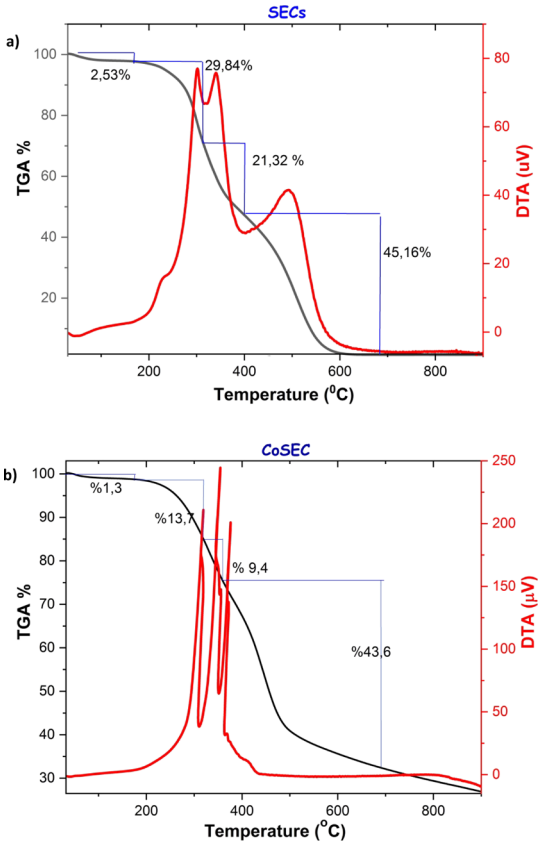

Figure 1. TGA/DTA analysis of (a) SECs and (b) CoSECs.

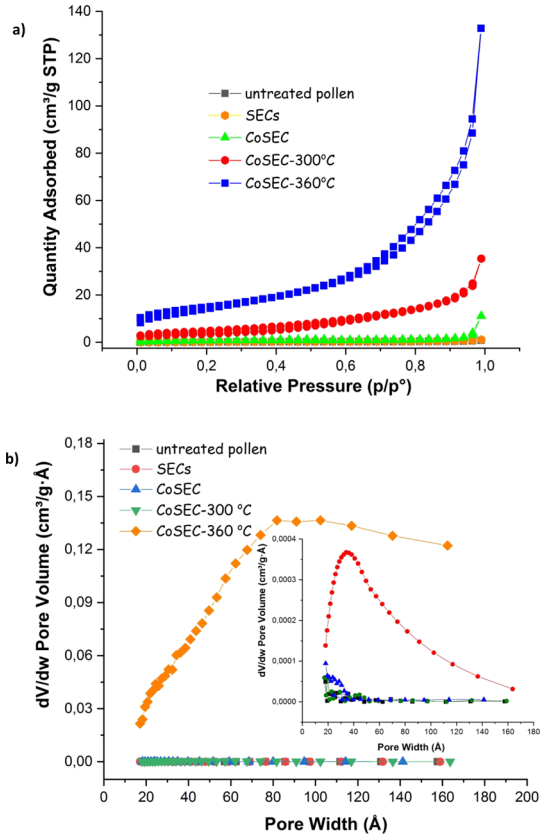

Figure 2. (a) N_2 adsorption/desorption isotherms and (b) pore distribution graphs for *Juglans* SECs that have undergone different processes.

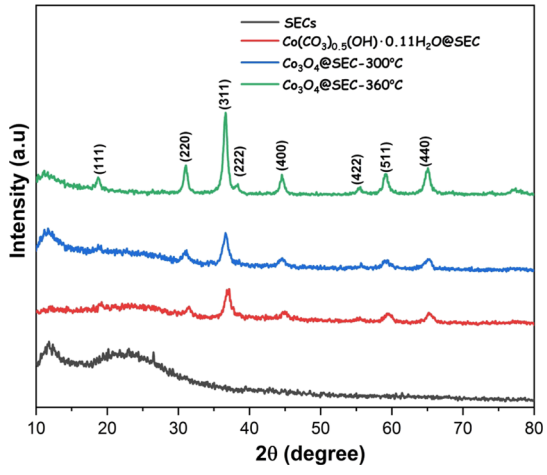

Figure 3. XRD spectra of *Juglans* SECs that have undergone different processes.

solutions to the aforementioned problems. Pollen or flower powders are substances with a protein structure that mediate the proliferation of flowering plants. Pollen grains are so small that they cannot be seen. In fact, a pollen powder can contain thousands of pollen grains. Every year, in certain seasons, different types of plants release their pollen to the environment during seasons with suitable temperature and humidity. While most tree pollen is dense in the atmosphere in late winter and early spring, grasses are found in spring and early summer. Also, weed pollen is more intense in late summer and autumn. Thus, it is possible to find plenty of pollen in nature in every season.

One of the main problems encountered during the production of nanostructured materials is that they tend to cluster, reducing their surface energy. To prevent this problem, growing the materials on a template is often desirable. These templates can be purpose-made membranes, produced by chemical methods, as well as known natural nanostructures. Nature already contains nanostructured materials of different sizes and shapes. For example, one-dimensional photonic structures and two-dimensional structures that are self-cleaning and have antireflective properties can appear in insect and butterfly wings or plant leaf flowers. Some studies suggest that morphological structures of cell walls and components of microorganisms, such as bacteria, viruses, algae, and fungi, can be good templates to produce nanostructures.[7−9] However, the production and purification of these microorganisms is a slow and difficult process, as we know from previous experience.[9,10]

Studies in the literature report that nanoparticles obtained using plant pollen can be used in areas such as drug transportation, catalysis, and wastewater treatment.[11−13] Pollen has been also used in biomedical applications as a microrobot, actuator, and sensor.[14−18] However, their use in energy technologies is limited.[11−13,19]

Pollen is a remarkable natural structure of the plant that carries genetic material to the female gamete.[20] Pollen consists of three main parts: cytoplasm, exine layer, and intine layer. The intine forms the inside of the pollen, adjacent to the cytoplasm, and carries the allergy-causing proteins. It is composed of cellulose, hemicelluloses, and pectin.[21,22] The exine structure is the outer part of the pollen, and taxonomically distinctive features are found on the exine structure. It is highly resistant to high temperature, various organic solvents, acids, alkalis, and

https://dx.doi.org/10.1021/acsomega.0c02355
ACS Omega 2020, 5, 20417−20427

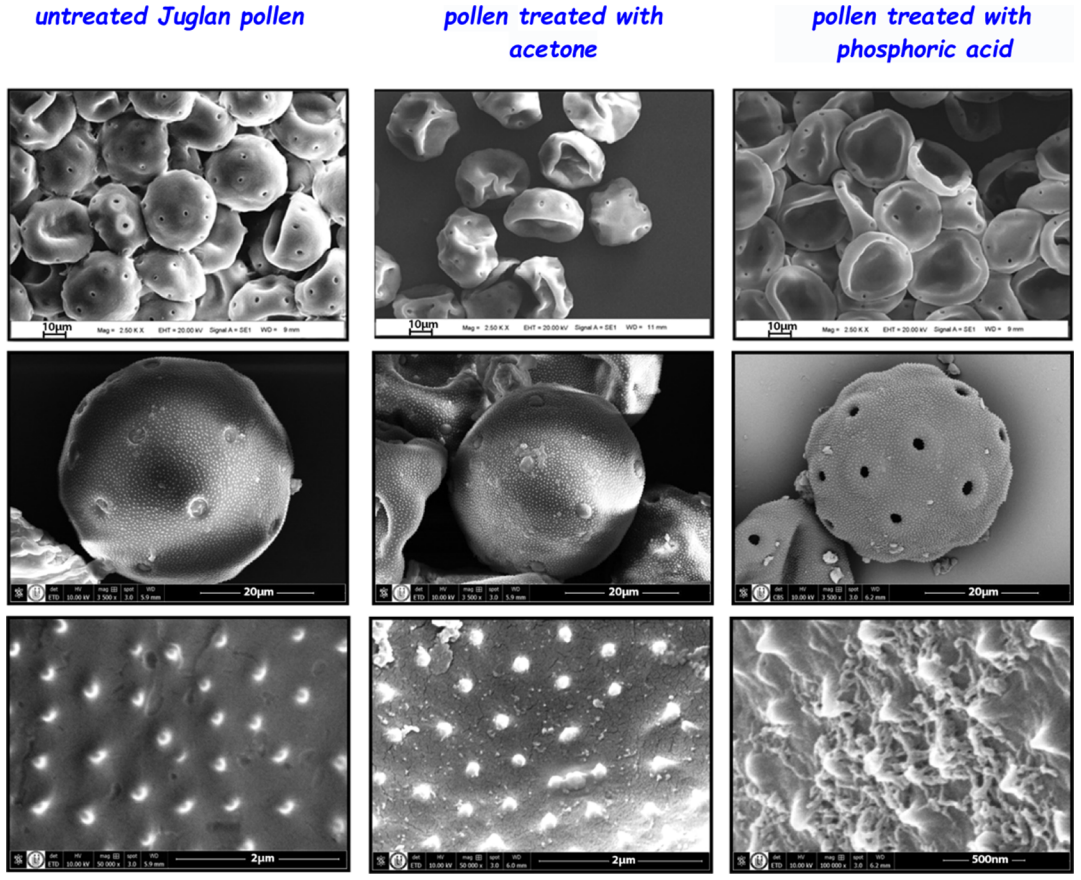

Figure 4. SEM images of untreated *Juglans* pollen, acetone-treated pollen, and phosphoric acid-treated pollen at different magnifications.

biodegradation.[23,24] The thin parts of the pollen tube located in this layer are called the aperture. The aperture is called a pore if it is in the form of holes and colpus if it is in the form of clefts. The number and location of the pores and colpi are one of the morphologically distinctive features of pollen. In addition to the apertures, there are ornaments consisting of pits and protrusions, called ornamentation, on the layer of the exine. These structures are among the most important criteria in the systematic identification of pollen.

The exine structure consists of a substance called sporopollenin, which is a polymer made up of small, aliphatic-organic monomer chains.[25−29] Spectroscopic analysis of the isolated sporopollenin shows that there are no polysaccharides and phenolic substances in the structure of the sporopollenin, and the carboxylic acid groups are bound by unsaturated bonds and ether bonds.[27] However, it has been determined that its chemical structure varies between species and development stages.[30,31] Zetzsche and Kälin[32] first defined the term sporopollenin as the material that forms the main part of the high resistance outer layer (exine) of pollen.[33] It is thought that these ionized functional groups on the sporopollenin exine microcapsule (SEC) surface will allow metal ligands to bind. Sporopollenins are the most durable materials of biological origin, which are resistant to both biological and chemical rot. In fact, after more than 500 million years, preserved sporopollenin was found in sedimentary rocks.[34] By applying sequential acidic and basic solvent processes, microcapsules can be obtained, which are free of cytoplasmic material, protein, and an intine layer and are protected from the exine layer.[35] Sporopollenin exine capsules are proper for applications including cell culture,[36] micromotor,[37] and drug delivery.[38]

Juglans pollen grain is spherical in shape and wind-pollinated. Its diameter varies between 33 and 40 μm. The spines found on the surface are longer than a micron (microechinate). The pollen grain has many pores on the exine (pantocolporate).[39] *Juglans* pollen grain has been preferred in this study because of its morphological structure and abundant pollen can be obtained easily by collecting catkins. When evaluated morphologically, it is assumed that the cytoplasmic content can be easily removed from the pores on its surface, and also the thorny structures on the surface will facilitate the attachment of the metal ligands to the surface, thereby increasing the surface area. In addition, as far as we know, studies on the production of nanostructured metal oxide coatings using *Juglans* pollen have not been found in the literature.

In this article, the production of hollow, porous, and nanostructured metal oxide/hydroxide materials and their use in energy storage will be investigated using nanostructured, three-dimensional (3D) sporopollenin microcapsules obtained from *Juglans* pollen. These pollen microcapsules will work as the most suitable biological substrates for producing mesoporous porous nanostructures and also cost-effective and environmentally benign.

RESULTS AND DISCUSSION

Thermogravimetric analysis (TGA) and differential thermal analysis (DTA) measurements of the SECs and hydrothermally cobalt-coated SECs are shown in Figure 1. The results show that the weight of the SECs was reduced during all four stages.

https://dx.doi.org/10.1021/acsomega.0c02355
ACS Omega 2020, 5, 20417−20427

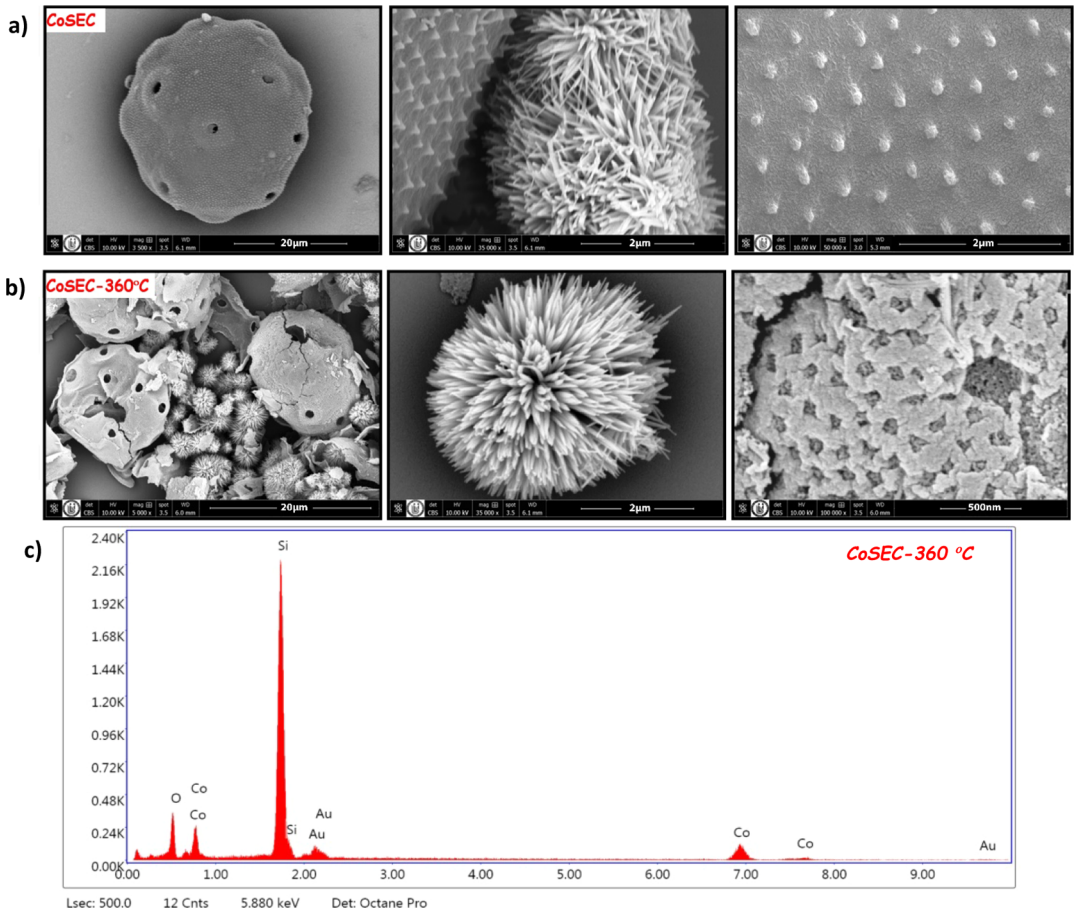

Figure 5. SEM images of (a) hydrothermally cobalt-coated SECs, (b) annealed at 360 °C at different magnifications, and (c) EDX analysis.

The loss in weight during the first stage, from room temperature to 170 °C, was approximately 2.53%. This can be attributed to the removal of absorbed water and humidity from the SEC surface. The second and third weight losses are attributed to the degradation of the residue of carbohydrates, proteins, and lipids, respectively. The carbonization takes place after approximately 620 °C. The weight losses after cobalt coating, in first and second steps, are similar to the SECs. However, the third and final degradation stages show that different phases of cobalt are formed. The amount of the remaining cobalt-based material was about 89.2 and 75.3% at 300 and 360 °C, respectively. These results indicate that the SECs constituted a significant part of the remaining material at 300 and 360 °C. The degradation of SECs with heating contributes to the weight loss of the samples. Also, this degradation partially changes the morphology of SECs. These changes can be seen in Figures S1 and S2 obviously. The TGA/DTA curve also illustrates that gradual decompositions of cobalt hydroxy carbonate to cobalt oxides and the degradation of the SECs occurred simultaneously in the temperature range of 319−360 °C, with a gradual weight loss of approximately 9.4%. The thermal decomposition reactions is

$$6[Co(CO_3)_{0.5}(OH)\cdot 0.11H_2O] + O_2 \rightarrow 3CO_2 + 3.66H_2O + 2Co_3O_4$$

The final mass loss step is observed at 800 °C and is attributed to the formation of CoO through loss of oxygen according to the reaction $2Co_3O_4 \rightarrow 6CoO + O_2$.

Figure 2a shows the adsorption and desorption isotherms of nitrogen at 77 K for the different sporopollenin-based powder materials. It is worth noting that, before the hydrothermal reaction, the Brunauer−Emmett−Teller (BET) specific surface area of the material was too small. BET surface area of pollen is decreased from 2.30 to 1.59 $m^2\ g^{-1}$ by the extraction process. The pore diameter also increased from 1.4 to 2.9 nm. This is an expected result. After the extraction process with acetone and acid, many micropores from the surface organic materials disappeared. The surface area value, which was calculated as 3.17 $m^2\ g^{-1}$ for the cobalt-coated material with the hydrothermal method, reached 17.41 and, then, 52 $m^2\ g^{-1}$ after heat treatments of 300 and 360 °C, respectively. The curve displays type four isotherm plots, according to IUPAC classification, which indicates mesoporous characteristics of the sample. The samples show a type H-tree hysteresis loop. This indicates that asymmetric, interconnected, slit-like mesoporosity existed in the samples. The pore size distributions of the prepared samples are shown in Figure 2b. The total pore volume also increased slightly from 0.000574 to 0.094 $cm^3\ g^{-1}$. The fact that a high micropore volume followed after the process provides evidence for the existence of nanostructured particles forming the pore walls.

Figure 3 shows the X-ray diffraction (XRD) pattern of the *Juglans* SEC-based samples with different treatments. The black spectrum belongs to SECs, and the red spectrum describes the hydrothermal-reacted SECs with cobalt and urea. The blue and green spectra belong to SECs that were hydrothermally treated and annealed at different temperatures. The broad peak at about

https://dx.doi.org/10.1021/acsomega.0c02355
ACS Omega 2020, 5, 20417−20427

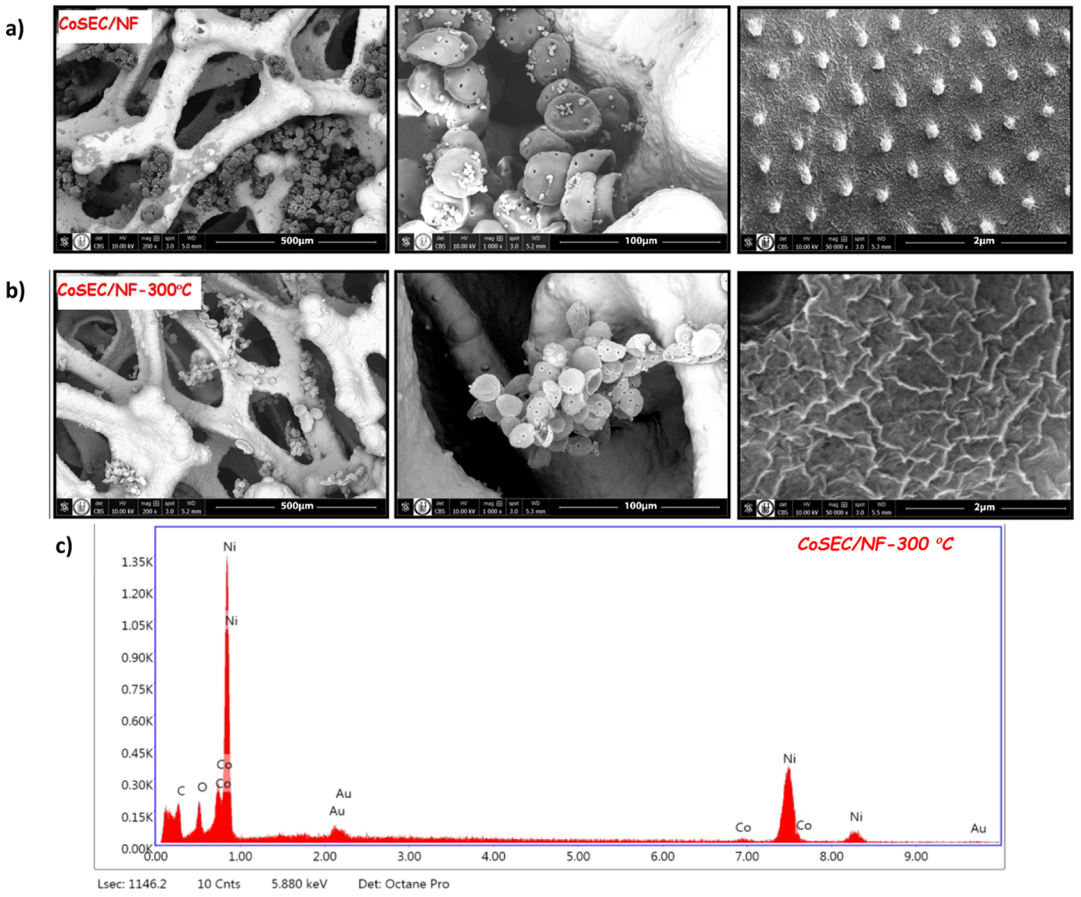

Figure 6. SEM images of (a) SECs coated with cobalt and adhered to Ni foam by a hydrothermal method, (b) annealed at 300 °C at different magnifications, and (c) EDX analysis.

23° indicates that the SECs are amorphous. $Co(CO_3)_{0.5}(OH)\cdot 0.11H_2O$ formation was obtained in hydrothermally-treated SECs. All of the identified peaks of hydrothermal cobalt-coated SECs can be assigned to pure orthorhombic $Co(CO_3)_{0.5}(OH)\cdot 0.11H_2O$, (JCPDS card number 48-0083). After the annealing process, the Co_3O_4 phase was obtained. It appears that the face-centerd Co_3O_4 phase was formed, with well-defined diffraction patterns indicating that they are crystalline. The diffraction peaks detected at 19.07, 31.30, 36.83, 38.5, 44.81, 55.63, 59.33, and 65.22° can be indexed as (111), (220), (311), (222), (400), (422), (511), and (440) planes, respectively (JCPDS, no. 43-1003). No other impurities were observed. Also, the broad XRD peaks of the 300 °C annealed sample exhibit nanocrystalline nature.

TGA/DTA curves have shown that starting from 300 °C, changes in the phase structure of the material have begun. In addition, XRD results showed that the cobalt hydroxy carbonate structure obtained after the hydrothermal treatment has a nanocrystalline structure at 300 °C, while the face-centered Co_3O_4 structure is formed at 360 °C. Based on these results and our previous experience,[40,41] temperatures of 300 and 360 °C were chosen as a annealing temperature. In addition, our BET measurements showed that the Co_3O_4 structure had the highest porosity at these temperatures.

Scanning electron microscopy (SEM) images of the raw *Juglans* pollen are shown in Figure 4. Raw pollen had nearly spherical, uniform morphology with a diameter of approximately 40 μm. The pollen surface has a very small, blunt, spiny structure and approximately 2 μm diameter pores where germination takes place. It was observed that, despite the sequential washing process with water and ethanol at least three times after the acetone treatment, the pollen had very small residues adhering to the surface, and also, the pores of the pollen were still clogged and swelling outward. After the orthophosphoric acid treatment, it was observed that the pollen surface was excessively eroded. The pores were completely opened, and the cytoplasm was removed from the pores. Through all of these chemical processes, the structural integrity of the SEC was not lost, and internal collapse had occurred. On the *Juglans* exine microcapsule, there are homogeneously structured spinies, approximately 100 nm high. These nano-spiny structures have served as nucleation and growth centers during the hydrothermal reaction. The thin nanostructured cobalt coating growing after the hydrothermal coating has completely covered the surface.

As seen from the high magnification images in Figure 5, the surface of the exine microcapsule was coated with Co_3O_4, and the desired porous structure on the pollen microcapsule that allowed for a high capacitance value was achieved. Compared to SEM images obtained from the heat-treated and untreated samples, the morphology of the microcapsules only changed slightly, but the surface structure of the microcapsules changed significantly. Particularly in the 360 °C heat-treated sample, the regular and porous coating on the pollen surface, as well as the spontaneous nano-thorn structure, is thought to have formed during the hydrothermal treatment, significantly contributing to the increase in surface area. The surface area of the nanostructured Co_3O_4 porous structure obtained after the heat treatment has increased 30 times approximately compared to

https://dx.doi.org/10.1021/acsomega.0c02355
ACS Omega 2020, 5, 20417−20427

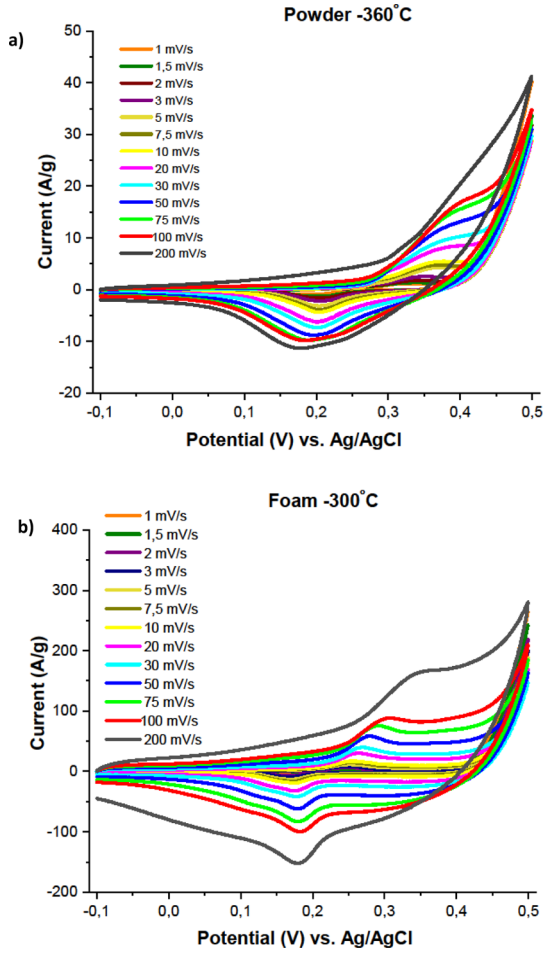

Figure 7. CV curves for the sporopollenin-based (a) CoSEC-360 and (b) CoSEC/NF-300 electrodes.

bare SEC. This increase is seen obviously from N_2 adsorption desorption graphs at Figure 2.

The hydrothermal process that was carried out in a closed environment in the liquid and at a low temperature provides an advantage over direct heat treatment. This process prevents the collapse of exine microcapsules partially. During hydrothermal treatment, the cobalt coating takes place simultaneously with a reduction in the SEC size. Thus, the strong structure grown on exine can be annealed to obtain the desired oxide phase.

If the metal ions were precipitated onto the pollen surface first and then heat-treated, this would lead to a significant change in the structure of the exine, such as the microstructure collapse and the cobalt layer delamination from the SEC surface. The partial collapse of SECs can pose important problems for drug delivery studies, but it is not so important for our studies.

The SEM and energy-dispersive X-ray (EDX) measurements after the hydrothermal cobalt coating and also heat treatments have shown that the whole surfaces of SECs were covered (Figures S2, 5). The EDX spectrum in Figure 5 was taken from the SEC surface. It has been found that the structures growing in the form of spherical nanothorny structures contain a higher rate of cobalt than the pollen surface. To see if the inside of the SECs were covered by cobalt during the hydrothermal reaction, SECs were cut with a surgical blade after liquid nitrogen application, as explained by Fan et al.[20] The SEM and EDX results have shown that the inside of the SECs are hollow with no trace of cobalt coating (Figures S3 and S4). It has also been found that the structures growing in the form of spherical nanothorny structures contain a higher rate of cobalt than the pollen surface.

The SEM images in Figure 6 show that both the Co_3O_4-coated SECs and Co_3O_4 nano-thorn structures adhered to the Ni foam. Hydrothermal treatment not only caused the formation of a nanoflake coating on the foam but also allowed the cobalt-coated SECs and nanothorns to adhere to the surface. This 3D network structure with different porous structures will be used directly as the supercapacitor electrode. This electrode, inevitably, shows high electrochemical performance.

A total of six different supercapacitor electrodes were prepared for two different electrode designs, in powder form or grown on foam at different heat treatment temperatures. Cyclic voltammetry (CV), measurements were taken in a three-electrode cell at room temperature using a leak free Ag/AgCl reference electrode and platinum counter electrode. CV measurements of the powder electrode and foam electrodes were taken in the potential range of −0.1 to 0.5 V and at different scanning rates (1−200 mV/s) in the 6 M KOH electrolyte (Figure 7). The best performances were observed in heat-treated samples at 360 °C for the powder electrode and 300 °C for the foam electrode; only the results of only these samples are included. The powder electrode was observed to operate at a lower current density than the foam electrode. It was also seen that the CV curves have similar shapes, and normalized peak currents increased with the increasing scan rate. These results indicate good reversibility of the fast charge−discharge (CD) response of both electrodes. The dominance of the pseudocapacitive behavior was also observed, which arose from the faradic reactions that occurred on the electrode surface. Also, it can be seen that the CV curves of the foam electrode are nearly rectangular in shape, which is desired in ideal supercapacitor electrodes.

The CD measurements were also performed in a three-electrode system by applying distinct current densities for testing the electrochemical capacitive feature of both electrodes. As seen in Figure 8, the hydrothermally grown structure on the foam electrode has better performance, in terms of allowing the supercapacitor electrode to work in a larger potential window and withstand higher current values. In addition, the specific capacitance values of the long term and consecutive, at least 1000, CD cycles for six different electrodes are shown in Figure 9, comparatively. Long-term galvanostatic CD measurements of the pollen-based electrodes for powder and foam were performed at currents of 2 and 5 A g^{-1}, respectively.

Specific capacitance (C) values were calculated for the long-term CD cycles using the formula below

$$C = \frac{I \times \Delta t}{m \times \Delta V} \quad (1)$$

where I was the discharge current, Δt was the discharge time, m was the mass of active material, and ΔV was the potential window.

The specific capacitance of the Co_3O_4-coated SEC-containing powder electrode (CoSEC) was 831 F g^{-1} initially, especially for the 360 °C heat-treated sample (CoSEC-360). This value quickly decreased to 472 F g^{-1} after 400 cycles. After 1000 cycles, the specific capacitance reached a minimum of 444 F g^{-1}. The maximum observed capacitance values in the untreated and heat-treated samples at 300 °C are 126 and 199 F g^{-1}, respectively, which are constant for almost 1000 cycles, as shown Figure 9a. Among the foam electrodes, the best result was observed in the heat-treated sample at 300 °C (CoSEC/NF-300, Figure 9b).

https://dx.doi.org/10.1021/acsomega.0c02355
ACS Omega 2020, 5, 20417−20427

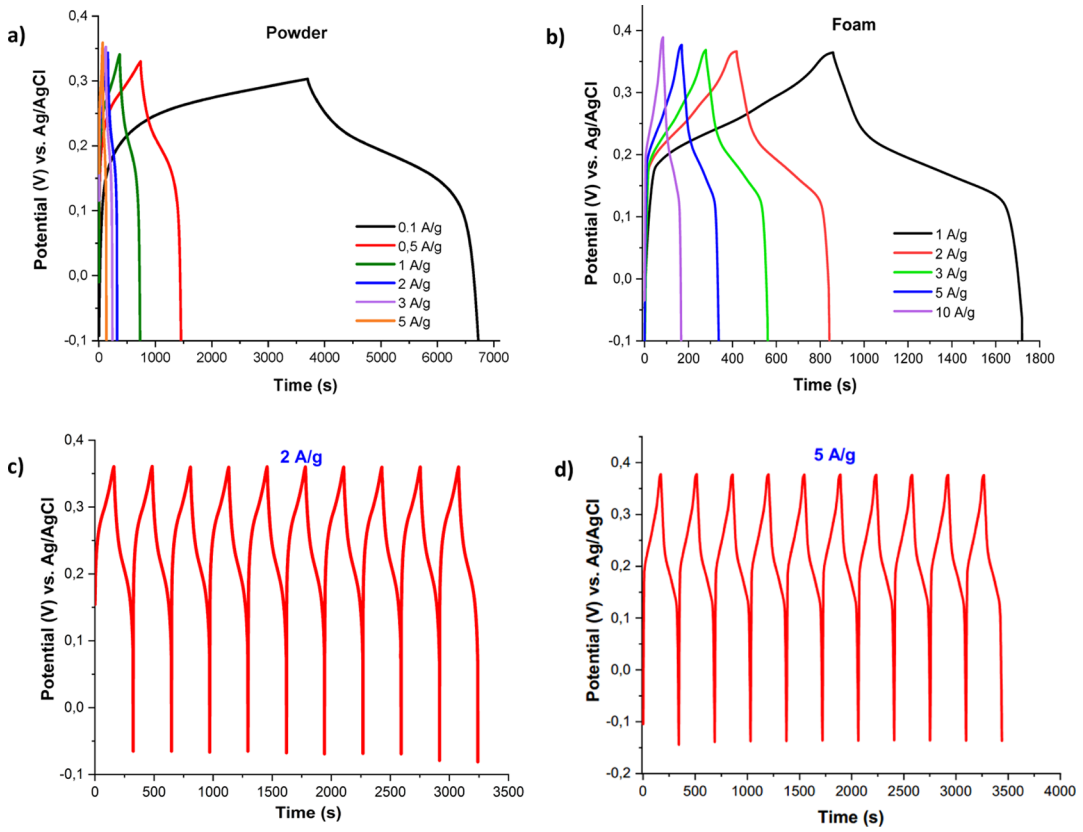

Figure 8. CD behaviors of sporopollenin-based electrodes at different current densities for (a) CoSEC-360 and (b) CoSEC/NF-300. The first 10 CD cycles for (c) CoSEC-360 at 2 A g^{-1} and (d) CoSEC/NF-300 at 5 A g^{-1} are shown.

The specific capacitance value increased from 1349 to 1512 F g^{-1} during the first 20 cycles and then reached a minimum of 1383 F g^{-1} in the 260th cycle and a maximum capacitance value of 1692 F g^{-1} after 1000 cycles. Specific capacitance values obtained for heat-treated CoSEC/NF at other temperatures are better than those observed for the best powder electrode. Thus, the change that occurs during the CD cycles on the electrode surface, as a result of 1000 cycles, does not limit the paths followed by electrons and ions. On the contrary, it allows diffusion to more internal regions for the heat-treated electrode at 300 °C and, also, contributes to the electrochemically active surface area. In the CoSEC/NF untreated and heat-treated samples at 360 °C, the maximum specific capacitance values initially observed are 804 and 324 F g^{-1}, respectively. These values decreased to 651 F g^{-1} for the untreated sample and 302 F g^{-1} for the 360 °C heat-treated sample after the first 20 cycles and, then, remained almost constant over 1000 cycles.

Electrochemical impedance spectroscopy studies were carried out for the CoSEC-360 and CoSEC/NF-300 electrodes, prepared under different conditions, between 100 kHz and 3 mHz and after both CV measurements and 1000 continuous CD cycles. The slope of the linear line in the high-frequency region for the CoSEC-360 powder electrode decreased from 71 to 54° after 1000 continuous CD cycles. For the CoSEC/NF-300 electrode, this value fell from 74 to 71°. As is known, for a supercapacitor, this value should be a minimum of 45°. The results show that both electrodes are good candidates for supercapacitor electrodes. Especially in the sample grown on the foam, there was almost no change in the load transfer resistance in the middle frequency region after long CD cycles. In addition, the initial electrode contact resistance for both electrodes did not change after prolonged cycles (Figure 9c).

Figure S5 has shown that the SECs were still well-standing on the surface and the 3D configuration maintained well after long-term CD cycles.

Also, a two-electrode asymmetric supercapacitor design was made to determine the device-level performance. The electrode including activated carbon (AC) was used as a cathode and the electrode based on CoSEC-300/NF was used as an anode. So, the working potential range of our asymmetric supercapacitor as a final device has been increased. Asymmetric CoSEC-300/NF//AC supercapacitor has exhibited maximum specific capacitance of 400 F g^{-1} at 5 A g^{-1} and stable capacitance retention of 95% after the 6000 cycles. The concerning results as added to the Supporting Information as Figure S6.

CONCLUSIONS

Juglans pollen surfaces have small, blunt, spiny structures. The spiny structures serve active metal-binding sites. Also, these sites allow the formation of new nucleation and growth centers (Figure S2d,f). Also, it is reported that if the hydrothermal reaction bath consists of urea, and is provided suitable conditions for pH, temperature, and concentration, nanothorny structures could be obtained.[42,43] Both spiny structures of SECs and also the hydrothermal process is happened a synergic effect to obtain porous and well-designed pollen-based electrodes. These nanothorny and spiny structures are also easily attached to foams. It is noteworthy that these superstructures are sufficiently stable, if it is used as a supercapacitor electrode, these problems observed in the powder electrode will not be seen. Pouring active mass from the electrode and swelling in the

https://dx.doi.org/10.1021/acsomega.0c02355
ACS Omega 2020, 5, 20417−20427

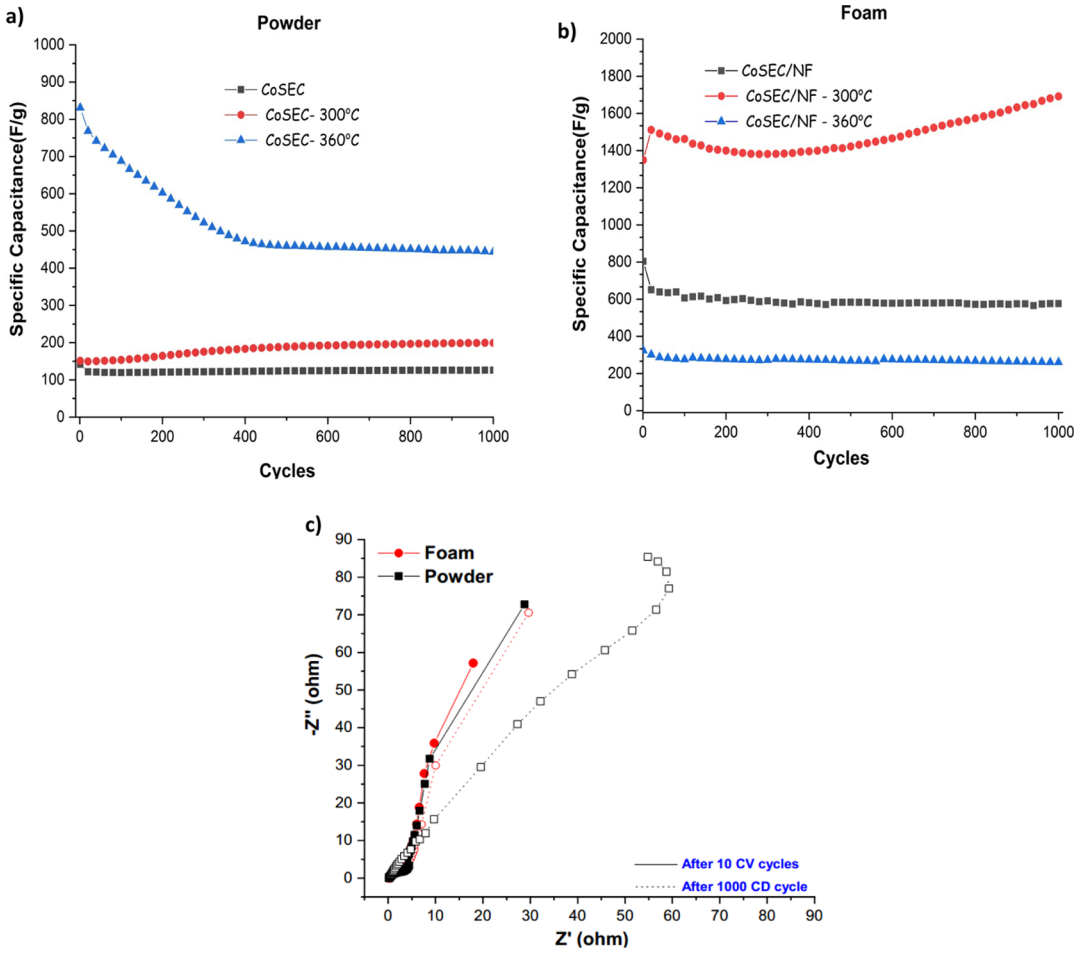

Figure 9. Specific capacitance of six different electrodes vs the number of CD cycles that have undergone different processes for (a) CoSEC and (b) CoSEC/NF. (c) Nyquist graph of both the fresh and cycled CoSEC and CoSEC/NF electrodes at an open-circuit potential.

polymer used as a binder in the electrode during CD cycling are the best-known problems. Also, mixing, grinding, and pressing processes will no longer be required for electrode production.

In summary, instead of using conventionally known production techniques, supercapacitor electrodes were produced by a different and easy method. The supercapacitor electrode design, with the use of exine microcapsules of *Juglans* sporopollenin, was tested for the first time. Both the SEC-based powder and foam electrodes exhibited good electrochemical stability and excellent capability rates. A very high value of specific capacitance (1692 F g^{-1}) was achieved.

EXPERIMENTAL SECTION

Juglans male flowers were picked up from different regions of Malatya, Turkey, and distinguished by dissection from their anthers. Isolation of pollen grains from anthers was carried out by sieving from suitable sieves (45−200 μm). *Juglans* SECs were separated from the intine and protoplasm by acetolysis with a reflux combination. Details of the SEC extraction processes can be found in our previous study.[14]

5 mM $Co(NO_3)_2{\cdot}6H_2O$ and 25 mM $CO(NH_2)_2$ were dissolved in pure ethanol, and the solution volume was increased to 100 mL by the addition of deionized water. Next, 75 mL of this solution was added to 0.3 g SECs. The resulting mixture was continuously stirred for 1 h, and then, it was poured into Teflon-lined stainless-steel cups with a capacity of 100 mL. The sealed cups were subjected to a hydrothermal reaction at 150 °C for 2 h. After the hydrothermal reaction, the remaining solution was centrifuged and, then, washed twice with water and ethanol. The obtained precipitate was dried in a vacuum oven at 60 °C for 12 h. Later, the precipitate was annealed in air atmosphere at 300 °C for 2 h. The obtained material, in a powder form, was used as the supercapacitor electrode active material. Cobalt-based powder (75%), which we obtained by the hydrothermal method, was mixed with acetylene black (15%) and poly(vinylidene difluoride) (10%) in a glove box for 45 min in Zr_2O_3 agate mortar. The total mass was 5 mg. Then, 400 μL of NMP was added to this homogeneous mixture. This slurry mixture was dropped onto Ni foam and dried in a vacuum oven at 60 °C. The working electrodes were obtained by pressing Ni foam coated with active material under 5 MPa of pressure.

We also fabricated 3D metal-oxide structures on Ni foam for direct use as supercapacitor electrodes. While hydrothermally producing powder materials, disc-shaped Ni foam pieces, 13 mm in diameter, were also added to Teflon-lined stainless-steel containers. The 3D nanostructured material on the Ni foam was directly used as a supercapacitor electrode. Both powder and 3D materials were used as electrode materials, first without annealing, and, then, after annealing at two different temperatures: 300 and 360 °C. The steps used to synthesize the metal oxide material and, then, produce a supercapacitor electrodes are given systematically in Figure 10.

The raw pollen, SECs, and CoSECs and CoSEC/Ni foam were characterized using SEM, BET surface area analysis,

https://dx.doi.org/10.1021/acsomega.0c02355
ACS Omega 2020, 5, 20417−20427

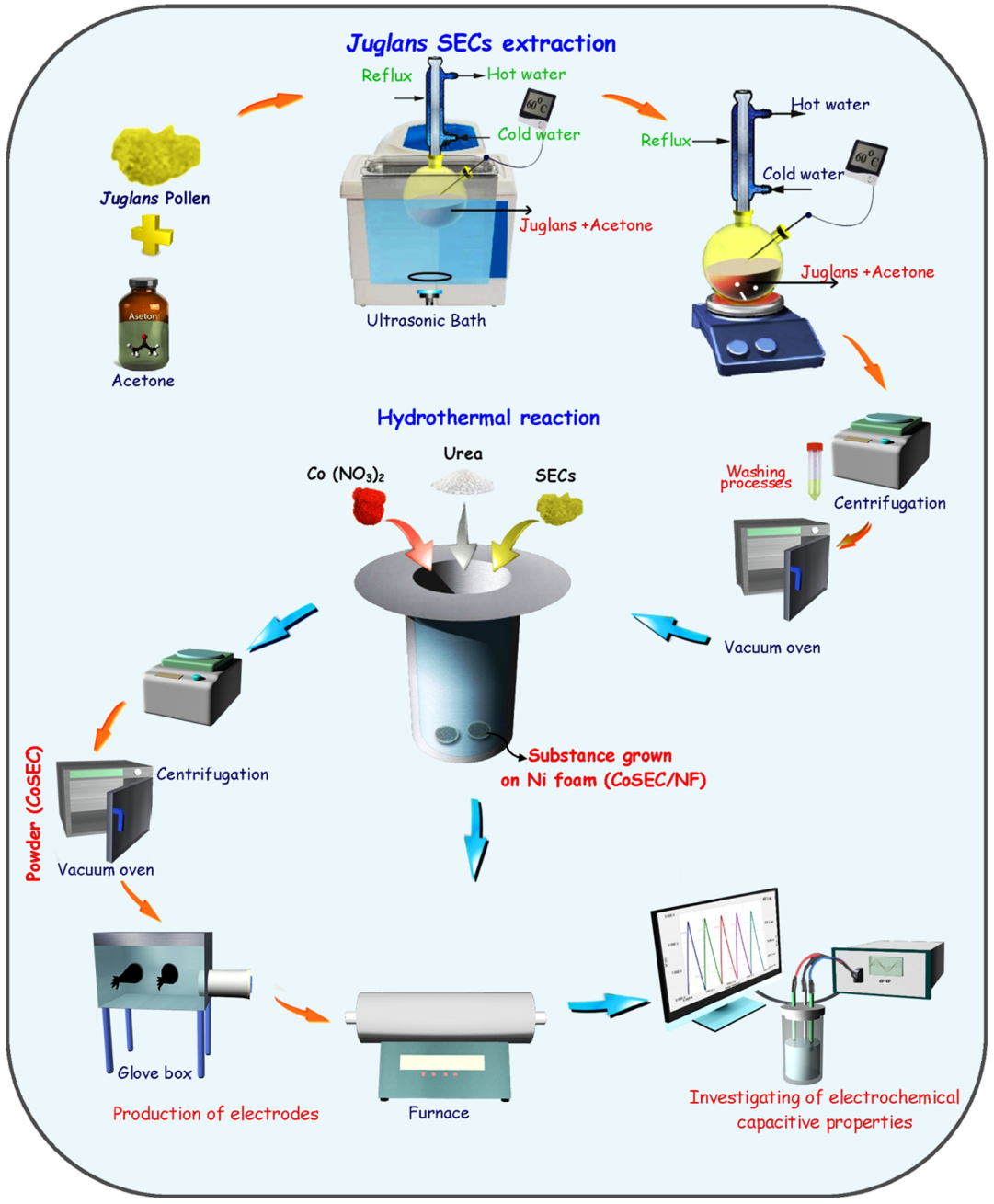

Figure 10. Systematic steps for creating differently designed electrodes with the sporopollenin content.

TGA/DTA, and XRD. The electrochemical performance was tested by CV, CD testing, and impedance spectroscopy techniques using a Gamry 3000 interface potentiostat/galvanostat/ZRA.

■ ASSOCIATED CONTENT

Supporting Information

The Supporting Information is available free of charge at https://pubs.acs.org/doi/10.1021/acsomega.0c02355.

Field emission SEM images of *Juglans* SECs bare SEC, annealed SEC at 300 °C, annealed SEC at 360 °C; cobalt-coated *Juglans* SECs after hydrothermal reactions (CoSEC), after the annealing process, CoSEC-300, CoSEC-360; Field emission SEM images of the inside of CoSEC after hydrothermal reaction; EDX spectrum of the inside of CoSEC after hydrothermal reaction; Field emission SEM images of the CoSEC/NF-300 electrode after the long term cycle test in the 6 M KOH electrolyte; electrochemical performance of the asymmetric CoSEC-300/NF//AC supercapacitor Galvanostatic first 10 CD curves, long term cycle stability at 5 A g^{-1}; and atomic force microscopy image of SEC (PDF)

■ AUTHOR INFORMATION

Corresponding Author

Funda Ersoy Atalay − *The Faculty of Science and Arts, Department of Physics, Inonu University, Malatya 44280, Turkey*; orcid.org/0000-0002-5776-2490; Email: funda.atalay@inonu.edu.tr

Authors

Alper Bingol − *The Faculty of Science and Arts, Department of Physics, Inonu University, Malatya 44280, Turkey*

https://dx.doi.org/10.1021/acsomega.0c02355
ACS Omega 2020, 5, 20417−20427

Harun Kaya − *The Faculty of Engineering and Natural Sciences, Malatya Turgut Ozal University, Malatya 44210, Turkey;* orcid.org/0000-0002-6090-0559
Yıldız Emre − *The Faculty of Science and Arts, Department of Physics, Inonu University, Malatya 44280, Turkey*
Hatice Hande Bas − *The Faculty of Science and Arts, Department of Physics, Inonu University, Malatya 44280, Turkey*
Ayse Asiye Culum − *The Faculty of Science and Arts, Department of Biology, Inonu University, Malatya 44280, Turkey*

Complete contact information is available at: https://pubs.acs.org/10.1021/acsomega.0c02355

Notes

The authors declare no competing financial interest.

■ ACKNOWLEDGMENTS

This work was supported by TUBITAK, project number 218M267, and by Inonu University BAP, project numbers 1709 and 2015/67.

■ REFERENCES

(1) Sun, Y.-F.; Liu, S.-B.; Meng, F.-L.; Liu, J.-Y.; Jin, Z.; Kong, L.-T.; Liu, J.-H. Metal oxide nanostructures and their gas sensing properties: A review. *Sensors* **2012**, *12*, 2610−2631.
(2) Zhang, X.; Guo, Q.; Cui, D. Recent advances in nanotechnology applied to biosensors. *Sensors* **2009**, *9*, 1033−1053.
(3) Lu, P.; Xue, D.; Yang, H.; Liu, Y. Supercapacitor and nanoscale research towards electrochemical energy storage. *Int. J. Smart Nano Mater.* **2013**, *4*, 2−26.
(4) de Jong, W. H.; Borm, P. J. A. Drug delivery and nanoparticles: Applications and hazards. *Int. J. Nanomed.* **2008**, *3*, 133−149.
(5) Wang, G.; Zhang, L.; Zhang, J. A review of electrode materials for electrochemical supercapacitors. *Chem. Soc. Rev.* **2012**, *41*, 797−828.
(6) Kang, Y.; Ye, X.; Chen, J.; Cai, Y.; Diaz, R. E.; Adzic, R. R.; Stach, E. A.; Murray, C. B. Design of Pt−Pd binary superlattices exploiting shape effects and synergistic effects for oxygen reduction reactions. *J. Am. Chem. Soc.* **2013**, *135*, 42−45.
(7) Mark, S. S.; Bergkvist, M.; Yang, X.; Teixeira, L. M.; Bhatnagar, P.; Angert, E. R.; Batt, C. A. Bionanofabrication of Metallic and Semiconductor Nanoparticle Arrays Using S-Layer Protein Lattices with Different Lateral Spacings and Geometries. *Langmuir* **2006**, *22*, 3763−3774.
(8) Shim, H.-W.; Jin, Y.-H.; Seo, S.-D.; Lee, S.-H.; Kim, D.-W. Reversible Lithium Storage in Bacillus subtilis-Directed Porous Co_3O_4 Nanostructures. *ACS Nano* **2011**, *5*, 443−449.
(9) Atalay, F. E.; Asma, D.; Kaya, H.; Ozbey, E. The fabrication of metal oxide nanostructures using *Deinococcus radiodurans* bacteria for supercapacitor. *Mater. Sci. Semicond. Process.* **2015**, *38*, 314−318.
(10) Atalay, F. E.; Asma, D.; Kaya, H.; Bingol, A.; Yaya, P. Synthesis of NiO Nanostructures Using *Cladosporium Cladosporioides* Fungi for Energy Storage Applications. *Nanomater. Nanotechnol.* **2016**, *6*, 28.
(11) Mundargi, R. C.; Potroz, M. G.; Park, S.; Shirahama, H.; Lee, J. H.; Seo, J.; Cho, N.-J. Natural Sunflower Pollen as a Drug Delivery Vehicle. *Small* **2016**, *12*, 1167−1173.
(12) Diego-Taboada, A.; Beckett, S. T.; Atkin, S. L.; Mackenzie, G. Hollow Pollen Shells to Enhance Drug Delivery. *Pharmaceutics* **2014**, *6*, 80−96.
(13) Dyab, A. K. F.; Abdallah, E. M.; Ahmed, S. A.; Rabee, M. M. Fabrication and Characterisation of Novel Natural *Lycopodium clavatum* Sporopollenin Microcapsules Loaded In-Situ with Nano-Magnetic Humic Acid-Metal Complexes. *J. Encapsulation Adsorpt. Sci.* **2016**, *06*, 109−131.
(14) Maric, T.; Nasir, M. Z. M.; Rosli, N. F.; Budanović, M.; Webster, R. D.; Cho, N. J.; Pumera, M. Microrobots Derived from Variety Plant Pollen Grains for Efficient Environmental Clean Up and as an Anti-Cancer Drug Carrier. *Adv. Funct. Mater.* **2020**, *30*, 2000112.
(15) Prabhakar, A. K.; Potroz, M. G.; Tan, E.-L.; Jung, H.; Park, J. H.; Cho, N.-J. Macromolecular Microencapsulation Using Pine Pollen: Loading Optimization and Controlled Release with Natural Materials. *ACS Appl. Mater. Interfaces* **2018**, *10*, 28428−28439.
(16) Prabhakar, A. K.; Potroz, M. G.; Park, S.; Miyako, E.; Cho, N. J. Spatially Controlled Molecular Encapsulation in Natural Pine Pollen Microcapsules. *Part. Part. Syst. Charact.* **2018**, *35*, 1800151.
(17) Wang, L.; Jackman, J. A.; Tan, E.-L.; Park, J. H.; Potroz, M. G.; Hwang, E. T.; Cho, N.-J. High-Performance, Flexible Electronic Skin Sensor Incorporating Natural Microcapsule Actuators. *Nano Energy* **2017**, *36*, 38−45.
(18) Zhao, Z.; Hwang, Y.; Yang, Y.; Fan, T.; Song, J.; Suresh, S.; Cho, N.-J. Actuation and Locomotion Driven by Moisture in Paper Made with Natural Pollen. *Proc. Natl. Acad. Sci. U.S.A.* **2020**, *117*, 8711−8718.
(19) Atalay, F. E.; Yigit, E.; Biber, Z. S.; Kaya, H. The Use of *Pistachio* Pollen for the Production of Nanostructured Porous Nickel Oxide. *Nano* **2018**, *13*, 1850143.
(20) Fan, T.-F.; Park, S.; Shi, Q.; Zhang, X.; Liu, Q.; Song, Y.; Chin, H.; Ibrahim, M. S. B.; Mokrzecka, N.; Yang, Y.; Li, H.; Song, J.; Suresh, S.; Cho, N.-J. Transformation of Hard Pollen into Soft Matter. *Nat. Commun.* **2020**, *11*, 1449.
(21) Fan, T.-F.; Hwang, Y.; Potroz, M. G.; Lau, K. L.; Tan, E. L.; Shahrudin Ibrahim, M.; Miyako, E.; Cho, N.-J. Degradation of the Sporopollenin Exine Capsules (SECs) in Human Plasma. *Appl. Mater. Today* **2020**, *19*, 100594.
(22) Fan, T.-F.; Potroz, M. G.; Tan, E. L.; Ibrahim, M. S.; Miyako, E.; Cho, N.-J. Species-Specific Biodegradation of Sporopollenin-Based Microcapsules. *Sci. Rep.* **2019**, *9*, 9626.
(23) Knox, R. B. The Pollen Grain. In *Embryology of Angiosperms*; Johri, B. M., Ed.; Springer Berlin Heidelberg: Berlin, Heidelberg, 1984; pp 197−271.
(24) Gonzalez-Cruz, P.; Uddin, M. J.; Atwe, S. U.; Abidi, N.; Gill, H. S. Chemical Treatment Method for Obtaining Clean and Intact Pollen Shells of Different Species. *ACS Biomater. Sci. Eng.* **2018**, *4*, 2319−2329.
(25) Pummer, B. G.; Bauer, H.; Bernardi, J.; Chazallon, B.; Facq, S.; Lendl, B.; Whitmore, K.; Grothe, H. Chemistry and Morphology of Dried-up Pollen Suspension Residues. *J. Raman Spectrosc.* **2013**, *44*, 1654−1658.
(26) Piffanelli, P.; Ross, J. H. E.; Murphy, D. J. Biogenesis and Function of the Lipidic Structures of Pollen Grains. *Sex. Plant Reprod.* **1998**, *11*, 65−80.
(27) Domínguez, E.; Mercado, J. A.; Quesada, M. A.; Heredia, A. Pollen sporopollenin: degradation and structural elucidation. *Sex. Plant Reprod.* **1999**, *12*, 171−178.
(28) Meuter-Gerhards, A.; Riegert, S.; Wiermann, R. Studies on Sporopollenin Biosynthesis in *Cucurbita maxima* (DUCH.) -II. The Involvement of Aliphatic Metabolism. *J. Plant Physiol.* **1999**, *154*, 431−436.
(29) Bubert, H.; Lambert, J.; Steuernagel, S.; Ahlers, F.; Wiermann, R. Continuous Decomposition of Sporopollenin from Pollen of *Typha angustifolia* L. by Acidic Methanolysis. *Z. Naturforsch., C: J. Biosci.* **2002**, *57*, 1035−1041.
(30) Hemsley, A. R.; Barrie, P. J.; Chaloner, W. G.; Scott, A. C. The Composition of Sporopollenin and its use in Living and Fossil Plant Systematics. *Grana* **1993**, *32*, 2−11.
(31) Meuter-Gerhards, A.; Schwerdtfeger, C.; Steuernagel, S.; Wilmesmeier, S.; Wiermann, R. Studies on sporopollenin structure during pollen development. *Z. Naturforsch., C: J. Biosci.* **1995**, *50*, 487−492.
(32) Zetzsche, F.; Kälin, O. Untersuchungen über die Membran der Sporen und Pollen V. 4. Zur Autoxydation der Sporopollenine. *Helv. Chim. Acta* **1931**, *14*, 517−519.
(33) Faegri, K.; Iverson, J. *Textbook of Pollen Analysis*; Blackwell Scientific Publications: Oxford, 1975; p 295.
(34) Brooks, J.; Shaw, G. *Origin and Development of Living Systems*; Academic Press: London and New York, 1973.
(35) Hamad, S. A.; Dyab, A. K. F.; Stoyanov, S. D.; Paunov, V. N. Sporopollenin microcapsules for microencapsulation of living cells. *MRS Proc.* **2013**, *1499*, 1−6.

(36) Tan, E.-L.; Potroz, M. G.; Ferracci, G.; Wang, L.; Jackman, J. A.; Cho, N.-J. Hydrophobic to Superhydrophilic Tuning of Multifunctional Sporopollenin for Microcapsule and Bio-Composite Applications. *Appl. Mater. Today* **2020**, *18*, 100525.
(37) Wang, H.; Potroz, M. G.; Jackman, J. A.; Khezri, B.; Marić, T.; Cho, N.-J.; Pumera, M. Bioinspired Spiky Micromotors Based on Sporopollenin Exine Capsules. *Adv. Funct. Mater.* **2017**, *27*, 1702338.
(38) Potroz, M. G.; Mundargi, R. C.; Gillissen, J. J.; Tan, E.-L.; Meker, S.; Park, J. H.; Jung, H.; Park, S.; Cho, D.; Bang, S.-I.; Cho, N.-J. Plant-Based Hollow Microcapsules for Oral Delivery Applications: Toward Optimized Loading and Controlled Release. *Adv. Funct. Mater.* **2017**, *27*, 1700270.
(39) Mert, C. Anther and Pollen Morphology and Anatomy in Walnut (*Juglans* Regia L.). *HortScience* **2010**, *45*, 757−760.
(40) Atalay, F. E.; Kaya, H.; Asma, D.; Bingol, A. Helical microtubules of nanostructured cobalt oxide for electrochemical energy storage applications. *Biointerface Res. Appl. Chem.* **2016**, *6*, 1099−1103.
(41) Yagmur, V.; Atalay, F. E.; Kaya, H.; Avcu, D.; Aydogmus, E. Electrochemical Capacitance of Cobalt Oxide Nanotubes on Nickel Foam. *Acta Phys. Pol., A* **2013**, *123*, 215−217.
(42) Ibupoto, Z. H.; Elhag, S.; AlSalhi, M. S.; Nur, O.; Willander, M. Effect of Urea on the Morphology of Co3O4 Nanostructures and Their Application for Potentiometric Glucose Biosensor. *Electroanalysis* **2014**, *26*, 1773−1781.
(43) Zhang, F.; Yuan, C.; Lu, X.; Zhang, L.; Che, Q.; Zhang, X. Facile growth of mesoporous Co3O4 nanowire arrays on Ni foam for high performance electrochemical capacitors. *J. Power Sources* **2012**, *203*, 250−256.

https://dx.doi.org/10.1021/acsomega.0c02355
ACS Omega 2020, 5, 20417−20427